Activation and Adsorption of Multiple H_2 Molecules on a Pd_5 Cluster: A Density Functional Study

Jerzy Moc,[†,‡] Djamaladdin G. Musaev,[*,‡] and Keiji Morokuma[*,‡]

Faculty of Chemistry, Wroclaw University, F. Joliot-Curie 14, 50-383 Wroclaw, Poland, and Cherry L. Emerson Center for Scientific Computation and Department of Chemistry, Emory University, Atlanta, Georgia 30322

Received: February 10, 2003

The density functional study of the activation and adsorption of several H_2 molecules on Pd_n clusters is extended to $n = 5$. Detailed mechanisms of H−H activation by the trigonal bipyramidal (tbp) Pd_5 cluster are described. They encompass various reaction pathways initiated by binding the first and second H_2 to the axial/equatorial atoms of the Pd_5 core, leading to the formation of $Pd_5(H)_2$ and $Pd_5(H)_4$ activation products, respectively. The $Pd_5 + H_2 \rightarrow Pd_5(H)_2$ reaction involves spin crossing, and the most stable product, which is a singlet, prefers both hydrogens at cap sites of the nonadjacent faces of Pd_5. By contrast to the cases for $n = 3$ and 4 studied previously, the activation of the second H_2 through the reaction $Pd_5(H)_2 + H_2 \rightarrow Pd_5(H)_4$ is found to be exothermic with an associated barrier (ΔH (298.15 K)) lying below the $Pd_5(H)_2 + H_2$ asymptote. The subsequent steps of the hydrogenation of Pd_5 take place via molecular adsorption onto the $Pd_5(H)_4$ dissociative complex, ultimately giving the hydrogen-rich cluster $Pd_5(H)_4(H_2)_5$, consistent with experiment. A comprehensive set of the non-hydrogen-saturated species that contain the $Pd_5(H)_4$ core structure have also been predicted. The thermodynamic stabilities of the $Pd_5(H)_4(H_2)_m$ ($m = 1-5$) hydrogenated clusters are discussed in terms of ΔH and ΔG values at $T = 298.15$ and 70 K.

I. Introduction

Hydrogen is forecast to be a principal source of energy in the future.[1] The use of molecular hydrogen as a fuel will result in a significant reduction of the emission of pollutant gases because H_2 is a cleanly burning fuel. In addition to producing vast quantities of inexpensive H_2, an important practical problem to be solved is that of safe and effective hydrogen storage.[1,2] It is known that metals, especially palladium, are excellent media for safe hydrogen storage.[2] From this viewpoint, detailed investigations of the interaction between bulk palladium surfaces and palladium clusters with H_2 molecules can contribute to designing useful hydrogen storage devices. Experimentally, it has been indicated that the palladium−hydrogen interaction and the quantity of adsorbed/absorbed hydrogen show a strong dependence on the metal surface and the size of the metal cluster.[3,4] From another perspective, hydrogen chemisorption is of vital technological importance to the industrial processes involving hydrogenation or dehydrogenation steps.[5] In general, small transition-metal clusters exhibit properties differing fundamentally from those of the corresponding bulk metal, as has been deduced from numerous gas-phase reactivity studies.[6] There are a plethora of examples in the literature illustrating the strong size dependence of the reactivity of both main group and transition-metal (TM) clusters, especially with molecular hydrogen.[4,6,7]

The present work contributes to our systematic theoretical studies of the reactivity of small palladium and platinum clusters toward H_2 and other small adsorbates. Previously,[8−10] we investigated the activation of the first H_2 (and CH_4) by Pt_n and Pd_n clusters for $n = 1-4$ using density functional theory (DFT) with the B3LYP functional and ab initio CASPT2 (complete active space second-order perturbation) methods. The B3LYP results were calibrated against the CASPT2 calculations and experimental data for $n = 1$ and 2.[8] It was proven that B3LYP yields reliable electronic structures as verified against the CASPT2 calculations and experimental data. In the preceding paper,[10] an extensive B3LYP study of the reactions of multiple H_2 molecules with the Pd_3 trimer and Pd_4 tetramer was carried out. In particular, for the $Pd_4 + H_2$ reaction, both singlet and triplet potential energy surfaces (PESs) were explored, and their crossing was indicated along the reaction coordinate. The singlet structure with the two H atoms bridging the nonadjacent Pd−Pd edges was predicted to be the most stable isomer of the $Pd_4(H)_2$ product. Unlike the first H_2 case, the activation of the second H_2 via reactions $Pd_3(H)_2 + H_2 \rightarrow Pd_3(H)_4$ and $Pd_4(H)_2 + H_2 \rightarrow Pd_4(H)_4$ appeared to be unfavorable.[10]

Here we extend our DFT study of the hydrogenation of the Pd_n clusters to $n = 5$. The sequential addition of H_2 molecules to the Pd_5 pentamer until saturation is examined in detail, including a multitude of the plausible hydrogenation intermediates. Special attention has been paid to the mechanisms of activation (dissociative adsorption) of the first several H_2 molecules by this TM cluster. To this end, the corresponding activation barriers and reaction profiles have been determined. The theoretical results are relevant to both the kinetic and saturation measurements of the chemisorption of H_2 and D_2 on the small gas-phase Pd_n clusters ($n < 25$) by Cox et al.[4] From the kinetic studies (low $H_2(D_2)$ pressure), these authors inferred a steady rise in the reaction rate between $n = 4$ and 8. In particular, the reaction of Pd_5 with $H_2(D_2)$ was indicated to proceed at a significantly higher rate than those of $Pd_{3,4} + H_2(D_2)$. On the basis of the saturation studies with D_2 (high D_2

* Corresponding authors. E-mail: morokuma@emory.edu. E-mail: dmusaev@emory.edu.
† Wroclaw University.
‡ Emory University.

10.1021/jp0343436 CCC: $25.00
Published on Web 05/23/2003

pressure), Cox et al. concluded that the resulting clusters were hydrogen rich, showing a D/Pd ratio significantly greater than 1. The above experiments[4] did not identify the hydrogenation intermediates.

II. Computational Methods

The methods of calculation followed those used in ref 10. Fully optimized structures and normal-mode frequencies were found using the B3LYP method[11] and relativistic effective core potential (ECP) of Hay and Wadt with the valence double-ζ (VDZ) basis set[12] on Pd in conjunction with DZ basis[13] for H (BSI). The energetics was improved by using the relativistic ECP of Dolg et al. on Pd and the associated valence triple-ζ basis sets[14] combined with Dunning's[15] augmented correlation-consistent basis for H (BSII). Spin-restricted and spin-unrestricted calculations were carried out for singlets and triplets, respectively. In the case of triplets, the alternation of the occupation numbers of the molecular orbitals was performed to ensure that the lowest-energy state was obtained. For reaction pathways, minima were connected to each transition state (TS) by tracing the intrinsic reaction coordinate (IRC).[16] Enthalpies and Gibbs free energies were calculated at both room temperature (298.15 K) and low temperature (70 K)[17] at 1 atm using vibrational frequencies evaluated at the B3LYP/BSI level. The Gaussian 98 quantum chemical package was used throughout.[18]

Recently,[10] we introduced the **Pdn_x_y_z** notation for the computed structures of the palladium/hydrogen clusters to systematize their description. Here, **n** is the number of TM atoms; **x** shows which H_2 molecule (first, second, etc.) enters the reaction; **y** describes the nature of the species, where **y** = **a**, **a′**,... corresponds to a dihydrogen complex, **y** = **b**, **b′**,... indicates the H−H activation transition state (TS), **y** = **c**, **c′**,... denotes the H−H activated product, and **y** = **d1**, **d2**,... is assigned to the isomerization TS; and **z** shows the position of the H ligands in the activated system. Within the activated system, the H ligand can (1) occupy the single (terminal) Pd atom, (2) bridge the edge of the Pd−Pd bond, or (3) cap the Pd−Pd−Pd face. These three binding sites are denoted **t**, **e**, and **f**, respectively. Furthermore, because the clusters calculated here have an even number of H ligands, **z** is going to have an even number of components. For instance, in the case of two H ligands, (**e,e**) indicates that they bridge two different Pd−Pd edges sharing the Pd atom, and (**e,e′**) shows that the two H ligands bridge two different Pd−Pd edges not sharing the Pd atom. Similarly, (**e,f**) indicates that the first H ligand bridges the Pd−Pd edge and the second one caps the Pd−Pd−Pd face, which shares the Pd atom or Pd−Pd edge, and (**e,f′**) relates to the situation when the bridging and cap sites do not share the Pd atom or Pd−Pd edge. Also, (**f,f**) shows both H ligands in cap sites that share the Pd−Pd edge and so on. Note that for four, six, and so forth H ligands, **z** is going to have four, six, and so forth components, respectively. For $n = 5$, we have added subscripts **ax** and **eq** to distinguish between the axial and equatorial Pd atoms shared or the axial and equatorial Pd−Pd edges shared, respectively.

III. Results and Discussion

Figure 1 shows optimized structures for the lowest singlet and triplet states of the bare Pd_5 cluster with the associated energetics included in Table 1. Species involved in activation of the first H_2 molecule on Pd_5 along with a number of singlet and triplet isomers of the $Pd_5(H)_2$ dissociative product are drawn in Figures 2 and 3. Their corresponding ΔH (298.15K) values are given in Figure 4. Species involved in the activation of the second H_2 molecule together with the various isomers of the $Pd_5(H)_4$ dissociative product are illustrated in Figure 5, and the related ΔH (298.15K) values are depicted in Figure 6. In turn, the structures of the energetically most favorable isomers of the third H_2 activation product, $Pd_5(H)_6$, and $Pd_5(H)_4(H_2)_m$ complexes for $m = 1-5$ are shown in Figure 7. Relative energies and thermodynamic values pertinent to the activation of the first, second, and third H_2 molecules are summarized in Tables 2 and 3. In Table 4, we have listed the relative energies and thermodynamic values of a large number of isomeric structures of the $Pd_5(H)_4(H_2)_m$ complexes for $m = 2-5$ with their structures presented in the Supporting Information (Figures 1S−4S). Finally, ΔH and ΔG values of the reactions $Pd_5(H)_4 + mH_2 \rightarrow Pd_5(H)_4(H_2)_m$ ($m = 1-5$) are presented in Figure 8.

Because the final energetics is determined with a basis set (BSII) that is larger than that used to calculate the geometries of the minima and transition states (BSI), it is possible that some apparent stationary points on the B3LYP/BSI PES might

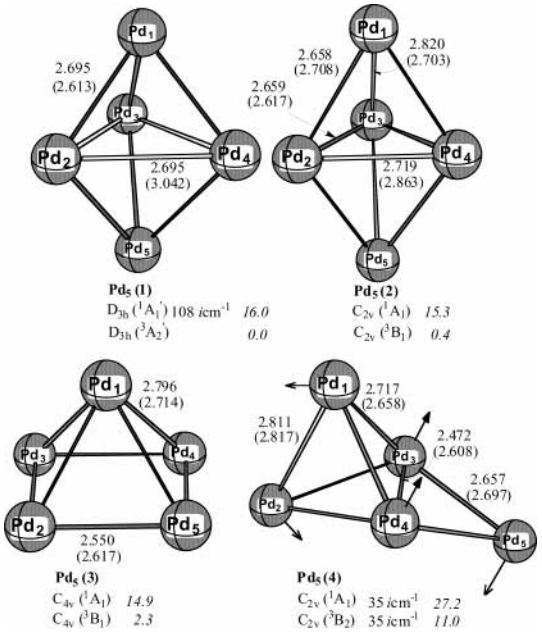

Figure 1. Optimized trigonal bipyramidal **Pd_5(1)**(D_{3h},$^1A_1'$,$^3A_2'$), distorted trigonal bipyramidal **Pd_5(2)**(C_{2v},$^1A_1$,$^3B_1$), square pyramidal **Pd_5(3)**(C_{4v},$^1A_1$,$^3B_1$), and edged-capped tetrahedron **Pd_5(4)** (C_{2v},$^1A_1$,$^3B_2$) structures of bare Pd_5 clusters (bond lengths in angstroms); distances in parentheses are for triplet states. The magnitude of the imaginary frequency for **Pd_5(1)**($^1A_1'$) and **Pd_5(4)**($^1A_1$,$^3B_2$) is included, together with the corresponding eigenvector for **Pd_5(4)** (essentially same for both $^1A_1$ and $^3B_2$). Values shown in italics are ΔH(298.15 K) relative to the ground-state triplet structure, $Pd_5(^3A_2')$(**Pd_5(1)**) (Table 1).

TABLE 1: Energies and Thermodynamic Values (kcal/mol) for Various Structures of the Bare Pd_5 Cluster Calculated at the B3LYP/BSII Level

			$T = 298.15$ K		$T = 70$ K	
structure[a]	ΔE	$\Delta E +$ ZPE	ΔH	ΔG	ΔH	ΔG
$Pd_5(^3A_2')$ (D_{3h}, **Pd_5(1)**)	0.0	0.0	0.0	0.0	0.0	0.0
$Pd_5(^1A_1')$ (D_{3h}, **Pd_5(1)**)	16.6	16.5	16.0	18.4	16.4	16.8
$Pd_5(^3B_1)$ (C_{2v}, **Pd_5(2)**)	0.4	0.4	0.4	0.5	0.4	0.4
$Pd_5(^1A_1)$ (C_{2v}, **Pd_5(2)**)	15.3	15.3	15.3	15.8	15.3	15.4
$Pd_5(^3B_1)$ (C_{4v}, **Pd_5(3)**)	2.2	2.7	2.3	3.9	2.6	2.8
$Pd_5(^1A_1)$ (C_{4v}, **Pd_5(3)**)	14.9	15.2	14.9	16.7	15.0	15.4
$Pd_5(^3B_2)$ (C_{2v}, **Pd_5(4)**)	11.5	11.9	11.0	13.2	11.7	11.9
$Pd_5(^1A_1)$ (C_{2v}, **Pd_5(4)**)	27.7	27.9	27.2	29.9	27.7	28.1

[a] See Figure 1 for the definition of structures.

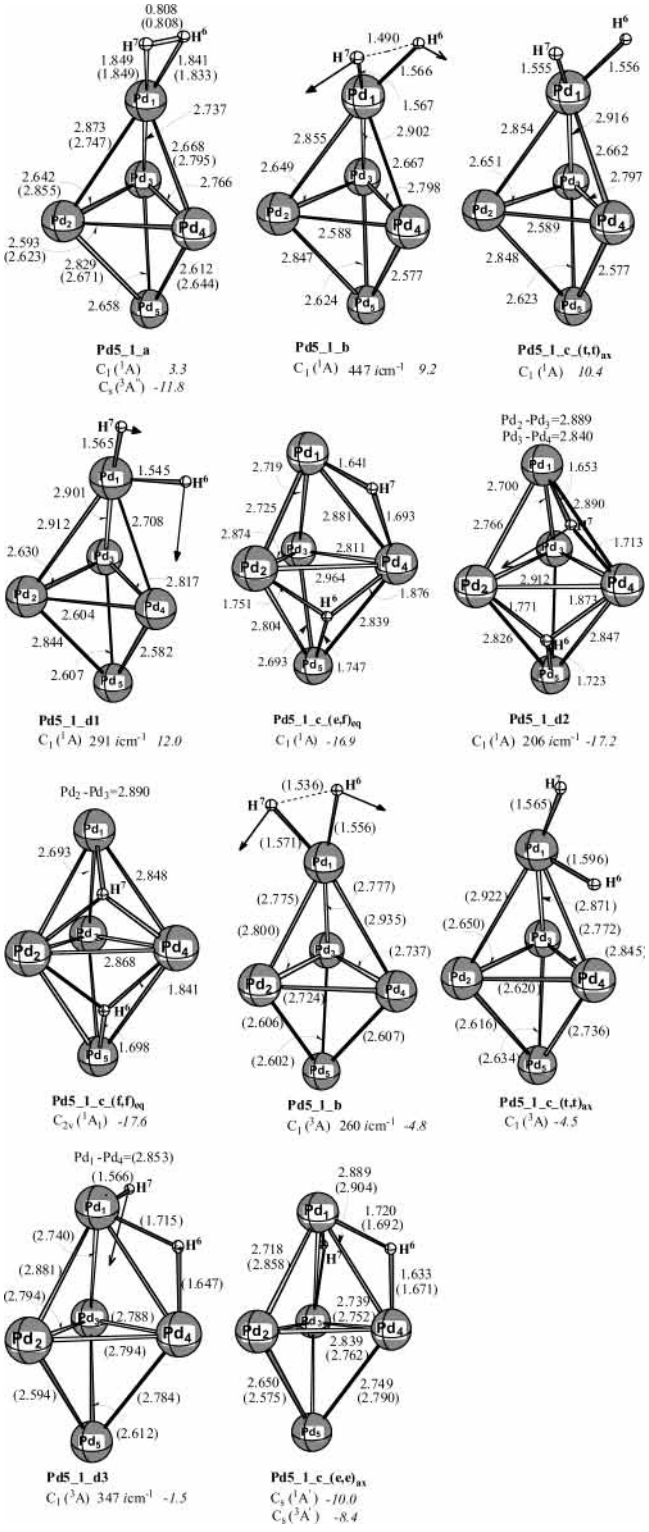

Figure 2. Optimized structures pertinent to the axial activation of the first H_2 on tbp Pd_5 proceeding through reaction $Pd_5 + H_2 \rightarrow Pd_5(H)_2$ and starting by H_2 attachment to the axial atom of the metal cluster (bond lengths in angstroms); distances in parentheses are for triplet states. Values shown in italics are ΔH(298.15 K) relative to the ground-state triplet reactants, $Pd_5(^3A_2')$(**Pd_5(1)**) + H_2 (Table 2). The reaction-coordinate vector and the corresponding imaginary frequency are shown for each TS.

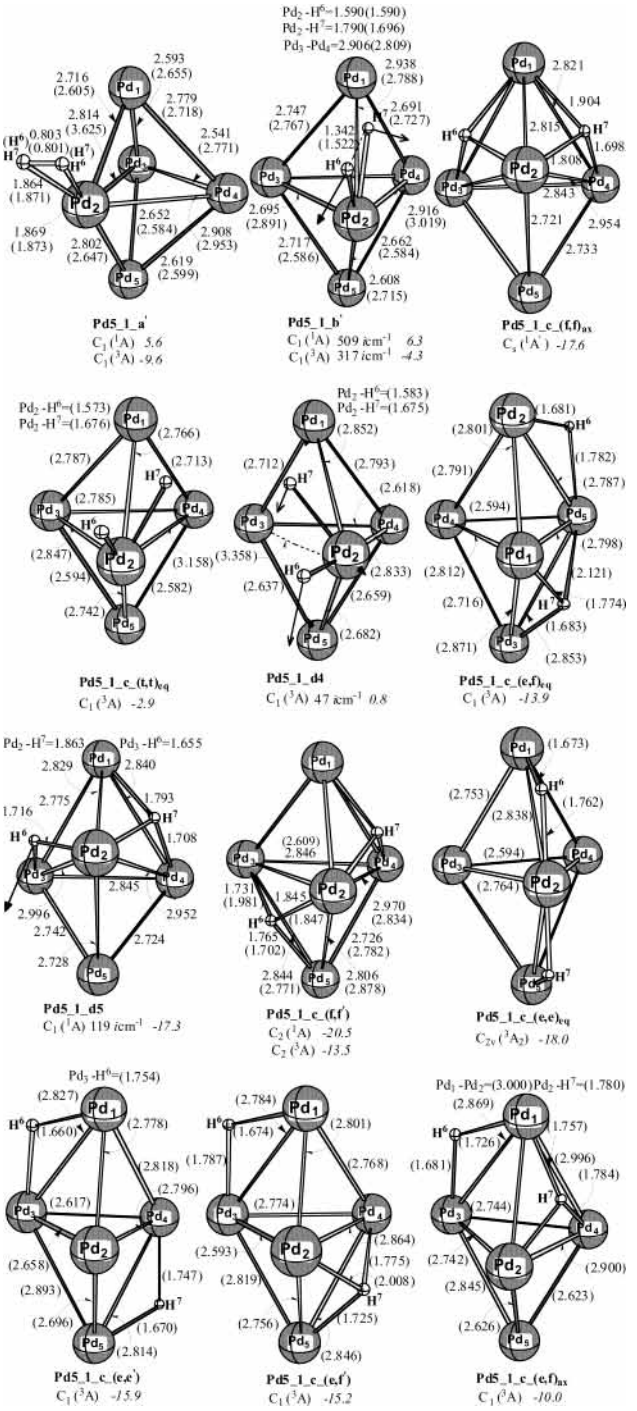

Figure 3. Optimized structures pertinent to the equatorial activation of the first H_2 on tbp Pd_5 proceeding through reaction $Pd_5 + H_2 \rightarrow Pd_5(H)_2$ and starting by H_2 attachment to the equatorial atom of the metal cluster, along with those of various $Pd_5(H)_2$ product isomers in singlet and triplet states (bond lengths in angstroms); distances in parentheses are for triplet states. Values shown in italics are ΔH(298.15 K) relative to the ground-state triplet reactants, $Pd_5(^3A_2')$(**Pd_5(1)**) + H_2. The reaction-coordinate vector and the corresponding imaginary frequency are shown for each TS.

disappear at the B3LYP/BSII//B3LYP/BSI level. These complications, encountered for some pathways of the $Pd_5 + H_2$ reaction (Figure 4), are commented on in section III.B.

A. Bare Pd_5 Cluster. The bare Pd_5 cluster was calculated earlier using B3LYP,[19,20] complete active space self-consistent-field (CASSCF), and multireference configuration interaction with single and double excitations (MRSDCI) methods.[21] Our results given in Figure 1 and Table 1 are consistent with the previously reported B3LYP results[19,20] and show that the triplet $^3A_2'$ state of the trigonal bipyramidal (tbp, D_{3h}) form of the Pd_5 cluster is the ground state. In the $^3A_2'$ state, the two unpaired electrons are occupying e″ orbitals. (The actual triplet symmetry was not determined in the previous B3LYP studies.) Another

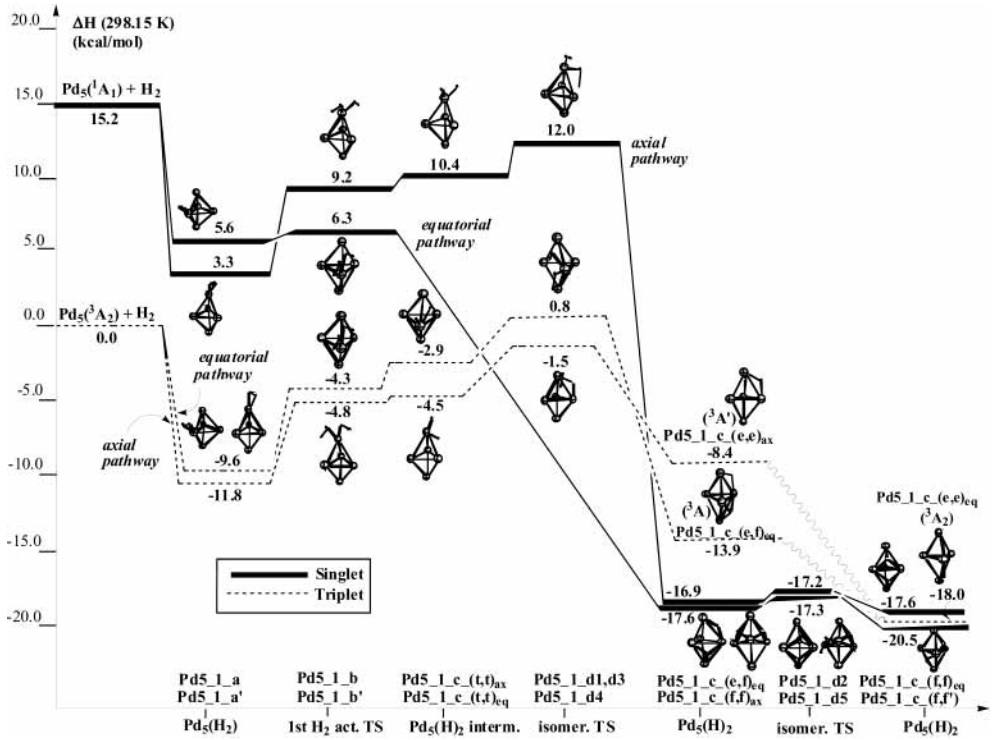

Figure 4. Profiles of ΔH(298.15 K) for activation of the first H_2 on tbp Pd_5.

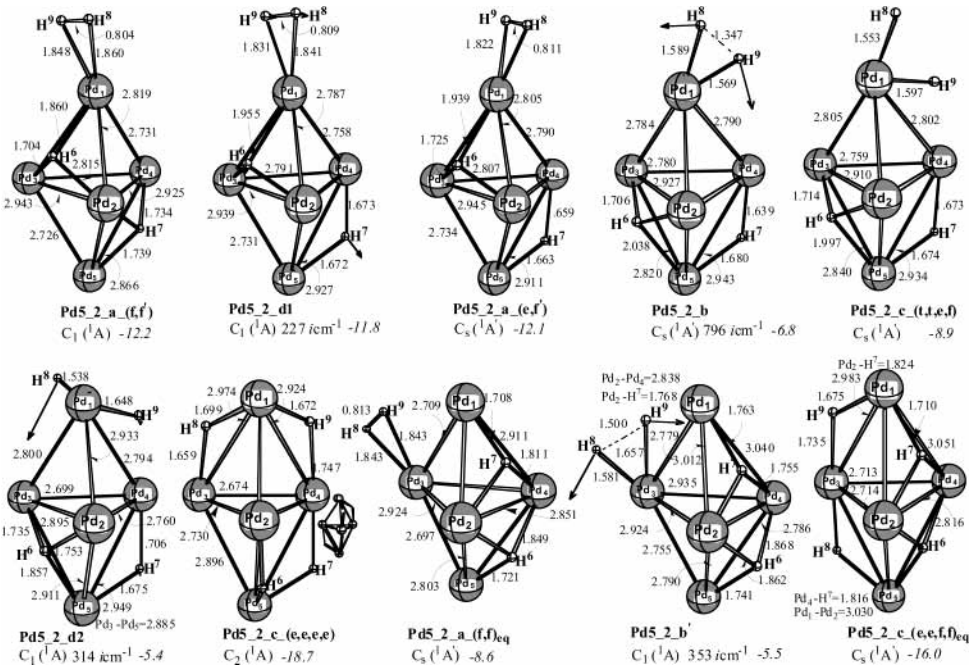

Figure 5. Optimized structures pertinent to the axial and equatorial activation of the second H_2 on tbp Pd_5 proceeding through reaction $Pd_5(H)_2 + H_2 \rightarrow Pd_5(H)_4$ and starting by H_2 attachment to the axial and equatorial Pd atoms of the Pd_5 core of $Pd_5(H)_2$, respectively (bond lengths in angstroms). Values shown in italics are ΔH(298.15 K) relative to the ground-state singlet reactants $Pd_5(H)_2$ (**Pd5_1_c_(f,f′)**) + H_2 (see Table 3). The reaction coordinate-vector and the corresponding imaginary frequency are shown for each TS.

triplet state, $^3B_1$, lies only 0.4 kcal/mol higher than $^3A_2'$ and is derived from the distorted tbp form of the Pd_5 cluster with C_{2v} symmetry (Table 1). These two low-energy triplet structures of Pd_5 are denoted as **Pd_5(1)**($^3A_2'$) and **Pd_5(2)**($^3B_1$), respectively, in Figure 1. As seen in this Figure, the triplet **Pd_5(1)**($^3A_2'$) features the "relaxed" equilateral triangle base with three sides of length 3.042 Å (the equatorial Pd−Pd edges) and six axial Pd−Pd edges of length 2.613 Å. In turn, **Pd_5(2)**($^3B_1$) exhibits the isosceles triangle base with the shorter (2.617 Å) and longer (2.863 Å) sides and axial edges of 2.703 Å. The regular tbp singlet **Pd_5(1)**($^1A_1'$) shows one imaginary frequency and distorts to C_{2v} symmetry (**Pd_5(2)**($^1A_1$). The lowest triplet state ($^3B_1$) of the square pyramidal (sp, C_{4v}) form of Pd_5, called **Pd_5(3)**($^3B_1$) in Figure 1, lies 2.3 kcal/mol above **Pd_5(1)**($^3A_2'$). The basal and apical Pd−Pd distances in **Pd_5(3)**($^3B_1$) are 2.617 and 2.714 Å, respectively. As seen in Figure 1 and Table 1, for all of the forms of Pd_5, the calculated singlet states lie significantly higher than the triplet states.[22] In particular, the singlet−triplet splitting of 15.3 kcal/mol found for the tbp-like structures is in good agreement with the earlier B3LYP estimate.[20]

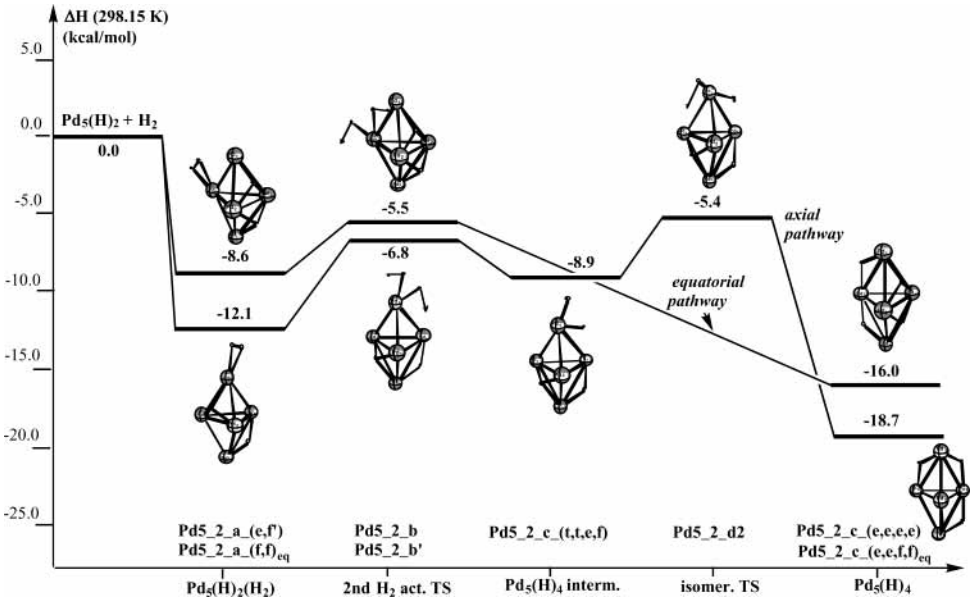

Figure 6. Profiles of ΔH(298.15 K) for activation of the second H_2 on $Pd_5(H)_2$.

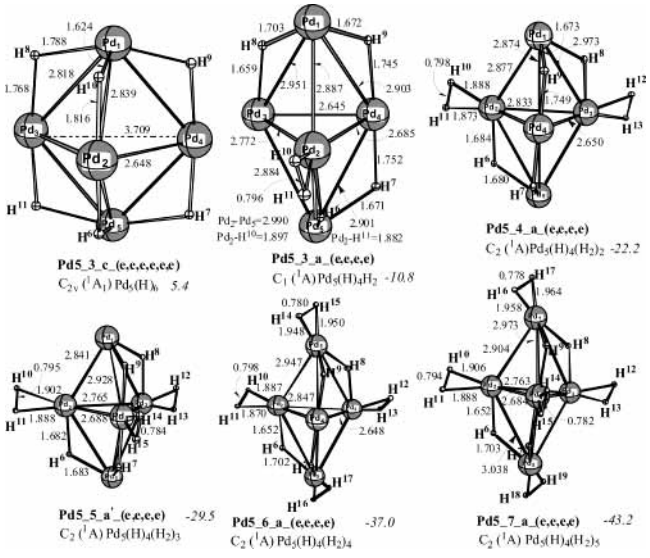

Figure 7. Optimized structures of the most stable $Pd_5(H)_4H_2$ complex, **Pd5_3_a_(e,e,e,e)**, and the most stable activation product, **Pd5_3_c_(e,e,e,e,e,e)**, of the activation of the third H_2 through the reaction $Pd_5(H)_4 + H_2 \rightarrow Pd_5(H)_6$. Also shown are optimized structures of the most stable $Pd_5(H)_4(H_2)_m$ ($m = 2-5$) complexes (bond lengths in angstroms). Values shown in italics are ΔH(298.15 K) relative to the most stable $Pd_5(H)_4$ (**Pd5_2_c_(e,e,e,e)**) + mH_2 reactants.

In the recent ab initio MRSDCI[21] study on Pd_5, seven different structures were examined using the LaJohn et al.[23] relativistic ECP. Consistent with our DFT B3LYP results, the tbp and sp forms of Pd_5 were predicted to be the lowest-energy structures (see below), and the C_{2v} edge-capped tetrahedron (ect) ($^3B_2$) structure was reported to be the third most favorable form of the Pd_5 cluster. The square (D_{4h}) planar, pentagonal (D_{5h}), and tetrahedral (T_d) structures of Pd_5 were found to be significantly higher in energy than the tbp and sp structures. (Consequently, these arrangements were not calculated in our studies.) Likewise, the planar trapezoidal C_{2v} structure was shown[21] to be energetically less favorable than the tbp and sp structures, and this result was confirmed by the B3LYP calculation (with this structure included in Supporting Information). In more detail, at the MRSDCI level, the three lowest-lying Pd_5 structures (states) were the tbp triplet ($^3E'$), sp singlet ($^1A_1$), and ect triplet ($^3B_2$), placed within 0.3 kcal/mol.[21]

Note that according to our results, ect **Pd_5(4)** ($^1A_1$ and $^3B_2$) (Figure 1) is not a minimum but rather a saddle point connecting the tbp-like structures on the singlet and triplet PESs, respectively. For instance, on the triplet PES, the B3LYP barrier for the Pd atom "scrambling" is found to be ca. 11 kcal/mol (Table 1).

B. Activation of the First H_2. From a hydrogen-activation point of view, the shape of the bare Pd_5 cluster is of importance. In addition to the energetic factor discussed in the preceding section, the use of the tbp-like Pd_5 isomer as a model for the activation of the first several H_2 molecules is justified by the known[8-10] inclination of H atoms (coming from the dissociated H_2) to occupy bridge sites on edges or cap sites on faces of the Pd_n polyhedron. Indeed, the tbp-like isomer of Pd_5 contains six triangular faces and nine edges (six axial and three equatorial), whereas the sp isomer possesses only five faces (four triangular and one square) and eight edges (Figure 1). Statistically, the former is expected to be more active toward such reactions than the latter. Therefore, we study below only the reaction of the tbp form of Pd_5 with H_2 molecules.

The $Pd_5 + H_2$ reaction starts by forming a dihydrogen complex $Pd_5(H_2)$. The H_2 molecule, being coordinated, can attach to the axial or equatorial sites of the tbp Pd_5. This gives rise to two distinct H_2 activation pathways (for each spin state) termed accordingly and described in detail below. First consider the axial coordination of the H_2 molecule and the resulting axial pathway. The H_2 coordination to the axial Pd atom results in the formation of the **Pd5_1_a** molecular complex (Figure 2) with the associated complexation enthalpy ΔH(298.15 K) of -11.8 (-11.9) kcal/mol for the triplet (singlet) state (Table 2). The corresponding values of the free energy of complexation ΔG(298.15 K) are -5.3 (-4.4) kcal/mol. Although the predicted ground state of **Pd5_1_a** is a triplet ($^3A''$) and the singlet state lies 15.2 kcal/mol higher in enthalpy (Table 2), we begin our discussion with the processes involving the singlet state. As seen in Figure 4, from the H_2 complex **Pd5_1_a**, the reaction proceeds via the axial transition state **Pd5_1_b** for H−H bond activation and leads to the dihydride intermediate **Pd5_1_c_(t,t)$_{ax}$**. The activation barrier calculated from **Pd5_1_a** is $\Delta H^{\ddagger}$(298.15 K) = 5.9 kcal/mol, and the transition state involved **Pd5_1_b** is located 6.0 kcal/mol below the $Pd_5(^1A_1) + H_2$ singlet asymptote (Table 2, Figure 4). The energy of this

TABLE 2: Energies and Thermodynamic Values (kcal/mol) for Species Involved in $Pd_5 + H_2$ Reactions Calculated at the B3LYP/BSII Level[a]

reaction species	ΔE	$\Delta E +$ ZPE	$T = 298.15$ K ΔH	$T = 298.15$ K ΔG	$T = 70$ K ΔH	$T = 70$ K ΔG
$Pd_5(^3A_2') + H_2$	0.0	0.0	0.0	0.0	0.0	0.0
$Pd_5(H_2)$ ($^3A''$) (**Pd5_1_a**)	−12.7	−10.9	−11.8	−5.3	−11.4	−10.1
axial first H_2 act. TS (^3A)(**Pd5_1_b**)	−3.9	−3.9	−4.8	1.4	−4.3	−3.1
$Pd_5(H)_2(^3A)$(**Pd5_1_c_(t,t)$_{ax}$**)	−4.3	−3.5	−4.5	2.6	−4.0	−2.6
isomer. TS (^3A) (**Pd5_1_d3**)	−0.7	0.0	−1.5	6.1	−0.5	0.8
$Pd_5(H)_2$ ($^3A'$)(**Pd5_1_c_(e,e)$_{ax}$**)	−8.4	−6.9	−8.4	−0.7	−7.4	−6.1
$Pd_5(^1A_1) + H_2$	15.2	15.2	15.2	15.3	15.2	15.2
$Pd_5(H_2)$ (**Pd5_1_a**)	2.3	4.3	3.3	10.9	3.8	5.3
axial first H_2 act. TS (**Pd5_1_b**)	10.0	10.4	9.2	17.2	9.9	11.4
$Pd_5(H)_2$ (**Pd5_1_c_(t,t)$_{ax}$**)	10.3	11.4	10.4	18.0	10.9	12.4
isomer. TS (**Pd5_1_d1**)	12.5	13.3	12.0	20.2	12.8	14.3
$Pd_5(H)_2$(**Pd5_1_c_(e, f)$_{eq}$**)	−16.7	−15.3	−16.9	−8.2	−15.9	−14.3
isomer. TS (**Pd5_1_d2**)	−16.2	−15.2	−17.2	−7.7	−15.8	−14.2
$Pd_5(H)_2$(**Pd5_1_c_(f,f)$_{eq}$**)	−17.0	−15.8	−17.6	−8.0	−16.3	−14.7
$Pd_5(H_2)$ (^3A)(**Pd5_1_a'**)	−10.6	−8.5	−9.6	−3.2	−9.0	−7.8
equatorial first H_2 act. TS (^3A)(**Pd5_1_b'**)	−3.1	−2.8	−4.3	3.5	−3.3	−2.0
$Pd_5(H)_2$ (^3A)(**Pd5_1_c_(t,t)$_{eq}$**)	−2.9	−1.6	−2.9	4.3	−2.1	−0.8
isomer. TS (^3A) (**Pd5_1_d4**)	1.5	2.5	0.8	9.4	2.0	3.4
$Pd_5(H)_2$ (^3A)(**Pd5_1_c_(e,f)$_{eq}$**)	−13.2	−12.5	−13.9	−6.5	−13.0	−11.7
$Pd_5(H_2)$(**Pd5_1_a'**)	4.7	6.5	5.6	12.8	6.0	7.5
equatorial first H_2 act. TS(**Pd5_1_b'**)	7.5	7.9	6.3	14.9	7.4	8.9
$Pd_5(H)_2$(**Pd5_1_c_(f,f)$_{ax}$**)	−16.8	−15.9	−17.6	−8.6	−16.5	−14.9
isomer. TS (**Pd5_1_d5**)	−16.3	−15.4	−17.3	−7.8	−15.9	−14.3
$Pd_5(H)_2$(**Pd5_1_c_(f,f')**)	−19.8	−18.7	−20.5	−11.0	−19.2	−17.6
$Pd_5(H)_2(^3A)$(**Pd5_1_c_(f,f')**)	−12.1	−12.0	−13.5	−5.4	−9.5	−7.7
$Pd_5(H)_2$(**Pd5_1_c_(e,e)$_{ax}$**)	−10.3	−8.5	−10.0	−1.4	−9.0	−7.5
$Pd_5(H)_2$ ($^3A_2$)(**Pd5_1_c_(e,e)$_{eq}$**)	−17.9	−16.4	−18.0	−9.3	−16.9	−15.4
$Pd_5(H)_2$ (^3A)(**Pd5_1_c_(e,e')**)	−15.7	−14.5	−15.9	−8.2	−15.0	−13.6
$Pd_5(H)_2$ (^3A)(**Pd5_1_c_(e,f')**)	−14.4	−13.6	−15.2	−7.2	−14.2	−12.8
$Pd_5(H)_2$ (^3A)(**Pd5_1_c_(e,f)$_{ax}$**)	−9.5	−8.4	−10.0	−2.2	−8.9	−7.6

[a] The species without state designations are closed-shell singlets (^1A).

TABLE 3: Energies and Thermodynamic Values (kcal/mol) for Species Involved in $Pd_5(H)_2 + H_2$ and $Pd_5(H)_4 + H_2$ Reactions Calculated at the B3LYP/BSII Level[a]

reaction species	ΔE	$\Delta E +$ ZPE	$T = 298.15$ K ΔH	$T = 298.15$ K ΔG	$T = 70$ K ΔH	$T = 70$ K ΔG
$Pd_5(H)_2$ (**Pd5_1_c_(f,f')**) + H_2	0.0	0.0	0.0	0.0	0.0	0.0
$Pd_5(H)_2(H_2)$(**Pd5_2_a_(f,f')**)	−13.3	−11.4	−12.2	−6.0	−11.8	−10.6
isomer. TS (**Pd5_2_d1**)	−12.7	−11.0	−11.8	−5.5	−11.4	−10.1
$Pd_5(H)_2(H_2)$(**Pd5_2_a_(e,f')**)	−13.8	−11.6	−12.1	−6.6	−12.0	−10.8
axial second H_2 act. TS(**Pd5_2_b**)	−6.5	−6.3	−6.8	−1.1	−6.7	−5.4
$Pd_5(H)_4$(**Pd5_2_c_(t,t,e,f)**)	−9.6	−8.1	−8.9	−2.3	−8.6	−7.2
isomer. TS (**Pd5_2_d2**)	−5.3	−4.0	−5.4	2.2	−4.5	−3.1
$Pd_5(H)_4$(**Pd5_2_c_(e,e,e,e)**)	−20.0	−17.2	−18.7	−10.3	−17.7	−16.2
$Pd_5(H)_2(H_2)$(**Pd5_2_a_(f,f)$_{eq}$**)	−9.5	−7.8	−8.6	−2.2	−8.3	−7.0
equatorial second H_2 act. TS(**Pd5_2_b'**)	−4.2	−4.3	−5.5	1.4	−4.7	−3.5
$Pd_5(H)_4$(**Pd5_2_c_(e,e,f,f)$_{eq}$**)	−16.4	−14.7	−16.0	−9.0	−15.1	−13.9
$Pd_5(H)_4$ (**Pd5_2_c_(e,e,e,e)**) + H_2	0.0	0.0	0.0	0.0	0.0	0.0
$Pd_5(H)_4(H_2)$(**Pd5_3_a_(e,e,e,e)**)	−12.0	−9.9	−10.8	−4.1	−10.3	−9.0
$Pd_5(H)_4(H_2)$(**Pd5_3_a'_(e,e,e,e)**)	−10.2	−8.1	−9.0	−1.9	−8.6	−7.2
$Pd_5(H)_4(H_2)$(**Pd5_3_a''_(e,e,e,e)**)	−9.3	−6.8	−7.7	−1.1	−7.3	−6.0
$Pd_5(H)_4(H_2)$(**Pd5_3_a_(e,e,e,f)**)	−9.3	−8.0	−8.7	−2.8	−8.3	−7.2
$Pd_5(H)_4(H_2)$(**Pd5_3_a_(e,e,f,f)$_{eq}$**)	−7.7	−6.9	−7.6	−2.5	−7.2	−6.2
$Pd_5(H)_4(H_2)$(**Pd5_3_a'_(e,e,f,f)$_{eq}$**)	−2.5	−1.7	−2.3	2.8	−2.1	−1.0
$Pd_5(H)_6$(**Pd5_3_c_(e,e,e,e,e,e)**)	6.1	7.5	5.4	15.4	7.0	8.6
$Pd_5(H)_6$(**Pd5_3_c_(e,e,f,f,f,f)**)	11.3	10.4	9.1	15.8	10.1	11.2

[a] The species without state designations are closed-shell singlets (^1A).

transition state relative to the ground-state $Pd_5(^3A_2') + H_2$ asymptote is 9.2 kcal/mol. With ΔG(298.15 K), the **Pd5_1_b** TS lies 1.9 kcal/mol above $Pd_5(^1A_1) + H_2$ and 17.2 kcal/mol above $Pd_5(^3A_2') + H_2$ (Table 2). In the next step, intermediate **Pd5_1_c_(t,t)$_{ax}$** isomerizes to the dihydride **Pd5_1_c_(e,f)$_{eq}$** via transition state **Pd5_1_d1**. The obtained edge−face singlet isomer of $Pd_5(H)_2$ can further isomerize to the more stable dihydride, **Pd5_1_c_(f,f)$_{eq}$**, through transition state **Pd5_1_d2** (Figures 2 and 4). We note that the last two connections involving the **Pd5_1_d1** and **Pd5_1_d2** transition states have been verified by tracing the IRC.[24a] The resulting **Pd5_1_c_(f,f)$_{eq}$** species has a structure of C_{2v} symmetry, where both H atoms cap the faces that share the equatorial Pd−Pd edge. It is 17.6 kcal/mol lower in enthalpy than the triplet reactants. In the capped sites of **Pd5_1_c_(f,f)$_{eq}$**, the Pd−H bond lengths are 1.698 and 1.841 Å.

TABLE 4: Energies and Thermodynamic Values (kcal/mol) for Species Involved in $Pd_5(H)_4 + mH_2$ ($m = 2-5$) Reactions Calculated at the B3LYP/BSII Level

			$T = 298.15$ K		$T = 70$ K	
reaction species[a]	ΔE	$\Delta E + \Delta$ZPE	ΔH	ΔG	ΔH	ΔG
$Pd_5(H)_4$ (**Pd5_2_c_(e,e,e,e)**) [$+mH_2$]	0.0	0.0	0.0	0.0	0.0	0.0
$Pd_5(H)_4(H_2)_2$(**Pd5_4_a_(e,e,e,e)**)	−24.6	−20.4	−22.2	−7.9	−21.3	−18.4
$Pd_5(H)_4(H_2)_2$(**Pd5_4_a′_(e,e,e,e)**)	−22.0	−17.8	−19.6	−5.9	−18.7	−16.0
$Pd_5(H)_4(H_2)_2$(**Pd5_4_a″_(e,e,e,e)**)	−21.0	−16.5	−18.3	−4.6	−17.4	−14.7
$Pd_5(H)_4(H_2)_2$(**Pd5_4_a‴_(e,e,e,e)**)	−20.9	−16.5	−18.2	−4.8	−17.4	−14.7
$Pd_5(H)_4(H_2)_2$(**Pd5_4_a$^{(4)}$_(e,e,e,e)**)	−19.0	−14.5	−16.2	−2.6	−15.3	−12.7
$Pd_5(H)_4(H_2)_2$(**Pd5_4_a_(e,e,f,f)$_{eq}$**)	−18.7	−15.9	−17.4	−4.9	−16.7	−14.2
$Pd_5(H)_4(H_2)_2$(**Pd5_4_a_(e,e,e,f)$_{eq}$**)	−15.1	−11.7	−13.3	−0.5	−12.5	−10.0
$Pd_5(H)_4(H_2)_2$(**Pd5_4_a′_(e,e,f,f)$_{eq}$**)	−13.6	−10.2	−11.8	0.6	−11.0	−8.5
$Pd_5(H)_4(H_2)_2$(**Pd5_4_a″_(e,e,f,f)$_{eq}$**)	−13.8	−11.2	−12.5	−0.9	−11.9	−9.5
$Pd_5(H)_4(H_2)_3$(**Pd5_5_a_(e,e,e,e)**)	−33.2	−26.7	−29.3	−8.8	−28.0	−23.9
$Pd_5(H)_4(H_2)_3$(**Pd5_5_a′_(e,e,e,e)**)	−33.2	−26.7	−29.5	−8.1	−28.1	−23.9
$Pd_5(H)_4(H_2)_3$(**Pd5_5_a″_(e,e,e,e)**)	−30.7	−24.2	−26.8	−6.2	−25.5	−21.4
$Pd_5(H)_4(H_2)_3$(**Pd5_5_a‴_(e,e,e,e)**)	−30.4	−23.5	−26.1	−5.7	−24.8	−20.7
$Pd_5(H)_4(H_2)_3$(**Pd5_5_a⁗_(e,e,e,e)**)	−27.9	−21.1	−23.7	−3.2	−22.4	−18.3
$Pd_5(H)_4(H_2)_3$(**Pd5_5_a_(e,e,f,f)$_{eq}$**)	−28.3	−22.8	−25.4	−5.5	−24.0	−20.1
$Pd_5(H)_4(H_2)_3$(**Pd5_5_a⁗′_(e,e,e,e)**)	−27.3	−21.4	−23.8	−3.9	−22.7	−18.7
$Pd_5(H)_4(H_2)_3$(**Pd5_5_a′_(e,e,f,f)$_{eq}$**)	−27.8	−23.1	−25.4	−6.6	−24.3	−20.6
$Pd_5(H)_4(H_2)_3$(**Pd5_5_a″_(e,e,f,f)$_{eq}$**)	−25.4	−20.6	−22.8	−4.7	−21.8	−18.1
$Pd_5(H)_4(H_2)_3$(**Pd5_5_a‴_(e,e,f,f)$_{eq}$**)	−24.5	−19.1	−21.6	−2.0	−20.3	−16.4
$Pd_5(H)_4(H_2)_4$(**Pd5_6_a_(e,e,e,e)**)	−42.6	−33.4	−37.0	−8.9	−35.2	−29.6
$Pd_5(H)_4(H_2)_4$(**Pd5_6_a′_(e,e,e,e)**)	−41.4	−32.5	−36.2	−8.0	−34.3	−28.8
$Pd_5(H)_4(H_2)_4$(**Pd5_6_a″_(e,e,e,e)**)	−39.3	−30.5	−33.9	−6.7	−32.2	−26.8
$Pd_5(H)_4(H_2)_4$(**Pd5_6_a_(e,e,f,f)$_{eq}$**)	−37.4	−30.2	−33.6	−6.8	−31.9	−26.6
$Pd_5(H)_4(H_2)_4$(**Pd5_6_a′_(e,e,f,f)$_{eq}$**)	−35.6	−28.2	−31.6	−5.4	−29.9	−24.7
$Pd_5(H)_4(H_2)_4$(**Pd5_6_a″_(e,e,f,f)$_{eq}$**)	−35.5	−28.0	−31.4	−4.9	−29.6	−24.4
$Pd_5(H)_4(H_2)_5$(**Pd5_7_a_(e,e,e,e)**)	−49.8	−38.9	−43.2	−8.2	−41.1	−34.1
$Pd_5(H)_4(H_2)_5$(**Pd5_7_a_(e,e,f,f)$_{eq}$**)	−45.1	−35.7	−40.0	−6.4	−37.8	−31.1

[a] If not indicated, the electronic state of the system is a closed-shell singlet.

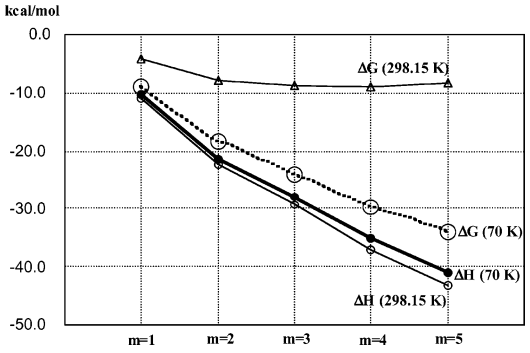

Figure 8. Profiles of ΔH(298.15 and 70 K) and ΔG(298.15 and 70 K) for the $Pd_5(H)_4 + mH_2 \rightarrow Pd_5(H)_4(H_2)_m$ ($m = 1-5$) reactions as functions of m. For each m, values for the most stable isomer of the $Pd_5(H)_4(H_2)_m$ complex are used.

Turning to the triplet axial pathway, complex **Pd5_1_a** ($^3A''$) goes over the **Pd5_1_b** (^3A) transition state and leads to the dihydride **Pd5_1_c_(t,t)$_{ax}$** (^3A) intermediate (Figures 2 and 4). Unlike the singlet counterpart, the H−H bond that is broken is positioned rather parallel to the Pd^1-Pd^4 edge within the **Pd5_1_b** (^3A) TS. This TS has a barrier of $\Delta H^{\ddagger}$(298.15 K) = 7.0 kcal/mol with respect to the initial dihydrogen complex, but is lower by 4.8 kcal/mol than the $Pd_5(^3A_2') + H_2$ asymptote. ΔG(298.15 K) places this TS ca. 1 kcal/mol above the latter asymptote (Table 2). The subsequent isomerization of the **Pd5_1_c_(t,t)$_{ax}$** (^3A) intermediate via the **Pd5_1_d3** transition state furnishes the **Pd5_1_c_(e,e)$_{ax}$** ($^3A'$) product as verified by the IRC calculation.[24a] The isomerization TS is located below the $Pd_5(^3A_2') + H_2$ reactants by 1.5 kcal/mol in terms of ΔH(298.15 K). The product **Pd5_1_c_(e,e)$_{ax}$** ($^3A'$) appears not to be the most stable $Pd_5(H)_2$ triplet species, as discussed in detail below. It is stabilized by 8.4 kcal/mol relative to $Pd_5(^3A_2') + H_2$, being 3.5 kcal/mol less stable in enthalpy than the initial **Pd5_1_a** ($^3A''$) complex.

Let us now consider the equatorial activation pathway, which begins with H_2 coordination to one of the Pd atoms forming the equatorial ring in the tbp Pd_5. This coordination mode results in the formation of the **Pd5_1_a′** complex (Figure 3) with −9.6 (−9.6) kcal/mol complexation enthalpy values at $T = 298.15$ K for the triplet (singlet) states. In terms of ΔG(298.15 K), these values are −3.2 (−2.5) kcal/mol (Table 2). The triplet complex is again found to be more stable (by 15.2 kcal/mol in enthalpy) than the singlet analogue. On the singlet PES, H_2 activation transforms the **Pd5_1_a′** initial complex directly to the **Pd5_1_c_(f,f)$_{ax}$** product through the equatorial transition state **Pd5_1_b′** (Figures 3 and 4). This has been verified by following the IRC. (Note that most of the structures in Figure 3 have been rotated relative to those in Figure 2 to get a better view of the Pd^2 equatorial active site and the ensuing $Pd_5(H)_2$ intermediates and products.) The **Pd5_1_b′** TS requires a calculated enthalpy of activation $\Delta H^{\ddagger}$(298.15 K) of only 0.7 kcal/mol from **Pd5_1_a′** and is 8.9 kcal/mol below the singlet asymptote. By using ΔG(298.15 K), the singlet **Pd5_1_b′** TS is found to lie 0.4 kcal/mol below $Pd_5(^1A_1) + H_2$ and 14.9 kcal/mol above $Pd_5(^3A_2') + H_2$ (Table 2). The product **Pd5_1_c_(f,f)$_{ax}$** shows both hydrogens at cap sites of the faces that share the axial edge and have the same binding enthalpy (17.6 kcal/mol) as **Pd5_1_c_(f,f)$_{eq}$** (Table 2). **Pd5_1_c_(f,f)$_{ax}$** can, however, easily isomerize to a more stable structure, **Pd5_1_c_(f,f′)**. The latter step comprises the movement of H^6 to the "nonshared" cap site, which is accomplished by **Pd5_1_d5** TS (cf. Figure 3). The resulting **Pd5_1_c_(f,f′)** isomer of C_2 symmetry with the two hydrogens occupying the nonadjacent faces appears to be the most stable structure of $Pd_5(H)_2$ and lies 20.5 kcal/mol below the ground-state reactants. In the cap sites, three Pd−H bonds of 1.731, 1.765, and 1.845 Å are formed. The closely related

edge−face and edge−edge singlet $Pd_5(H)_2$ isomers of the nonshared type, **Pd5_1_c_(e,f′)** and **Pd5_1_c_(e,e′)**, respectively (not shown in Figure 3), have been found to be kinetically unstable because the two collapsed to **Pd5_1_c_(f,f′)** after enforcing tighter geometry-optimization criteria.

Turning to the triplet equatorial pathway, we first note that the relatively weak equatorial Pd−Pd edge essentially breaks upon forming the **Pd5_1_a′** (^{3}A) molecular complex (with a Pd^2-Pd^3 distance of 3.625 Å). In the next step, activation of the H−H bond occurs via the equatorial transition state **Pd5_1_b′** (^{3}A), which connects the **Pd5_1_a′** (^{3}A) complex to the **Pd5_1_c_(t,t)$_{eq}$** (^{3}A) intermediate (Figures 3 and 4). This H_2 activation mode requires overcoming the $\Delta H^{\ddagger}$ (298.15 K) barrier of 5.3 kcal/mol relative to **Pd5_1_a′** (^{3}A), but most importantly, the **Pd5_1_b′** (^{3}A) TS lies 4.3 kcal/mol below the triplet reactants (Figure 4).[24b] The follow-up rearrangement of the **Pd5_1_c_(t,t)$_{eq}$** (^{3}A) intermediate via the **Pd5_1_d4** (^{3}A) TS yields the **Pd5_1_c_(e,f)$_{eq}$** (^{3}A) product. The corresponding transition structure **Pd5_1_d4** (^{3}A) is located just 0.8 kcal/mol above the $Pd_5(^3A_2')$ + H_2 asymptote (Figure 4). This complex rearrangement involves (1) pseudorotation of the Pd_5 cluster skeleton accompanied by the successive equatorial ring Pd^2-Pd^3 bond breaking and Pd^1-Pd^5 bond forming and (2) movement of both terminal hydrogens to the more preferred bridge and cap binding sites. As a result of (1), the pairs of axial and equatorial Pd atoms in the **Pd5_1_c_(e,f)$_{eq}$** (^{3}A) product are interchanged relative to those in the **Pd5_1_c_(t,t)$_{eq}$** (^{3}A) intermediate (cf. Figure 3). The **Pd5_1_c_(t,t)$_{eq}$** (^{3}A) → **Pd5_1_c_(e,f)$_{eq}$** (^{3}A) rearrangement has been verified by following the IRC from **Pd5_1_d4** TS.[24c] The triplet product **Pd5_1_c_(e,f)$_{eq}$** (^{3}A) is stabilized by 13.9 kcal/mol (ΔH(298.15 K)) with respect to $Pd_5(^3A_2')$ + H_2. This is 3.0 kcal/mol less than the value obtained for the singlet analogue discussed above.

A similar situation is true for the other $Pd_5(H)_2$ structures located for both spin states. For instance, the triplets **Pd5_1_c_(f,f′)** (^{3}A) and **Pd5_1_c_(e,e)$_{ax}$** (^{3}A′) (Figures 2 and 3) are predicted to be 7.0 and 1.6 kcal/mol, respectively, less stable in ΔH (298.15 K) than their singlet counterparts.[25] However, our extensive exploration of the triplet PES revealed additional low-energy $Pd_5(H)_2$ isomers that did not exist in the singlet state and show unique geometries. They are labeled **Pd5_1_c_(e,e)$_{eq}$** ($^3A_2$), **Pd5_1_c_(e,e′)** (^{3}A), **Pd5_1_c_(e,f′)** (^{3}A), and **Pd5_1_c_(e,f)$_{ax}$** (^{3}A) in Figure 3. These calculations also found that the "shared" edge−edge structure, **Pd5_1_c_(e,e)$_{eq}$** ($^3A_2$), is the lowest triplet state of $Pd_5(H)_2$. This is different from the lowest singlet state of $Pd_5(H)_2$ as well as $Pd_4(H)_2$ and $Pd_3(H)_2$,[9,10] all having the nonshared structures. According to our calculations, the lowest triplet isomer of $Pd_5(H)_2$ is only 2.5 kcal/mol less stable than the Pd_5H_2 global minimum, the singlet **Pd5_1_c_(f,f′)** (Table 2). We recall here that for $Pd_4(H)_2$ the most favorable triplet isomers were higher in enthalpy by ca.10 kcal/mol compared to the singlet isomers.[10] The analysis of the spin-density distribution in **Pd5_1_c_(e,e)$_{eq}$** ($^3A_2$) assigns 54% of the two unpaired electrons to the equatorial Pd atoms not involved in the Pd−H bond and 43% to the axial Pd atoms, with the remaining 3% delocalized onto the third equatorial Pd and both hydrogens. The isomerization of the **Pd5_1_c_(e,f)$_{eq}$** (^{3}A) activation product to form **Pd5_1_c_(e,e)$_{eq}$** ($^3A_2$) is anticipated[8−10] to be a low-barrier process and has not been pursued further.

In search of the other (possibly barrierless) possibilities for the single H_2 approaching the tbp Pd_5 and leading to $Pd_5(H)_2$, various pathways have also been considered for the singlet state. More specifically, the equatorial−perpendicular, axial−perpendicular, equatorial−parallel, and axial−parallel modes under C_{2v} and C_s symmetry were examined as summarized in the Supporting Information. None of these routes appeared to be more favorable than those already discussed.

On the basis of the potential energy profiles given in Figure 4, one may conclude that the Pd_5 + H_2 reaction starts with the triplet-state reactants and proceeds along either the axial or equatorial pathways. Because the H−H activation TS lies 4 to 5 kcal/mol lower than the Pd_5 + H_2 reactants, no overall enthalpy barrier is found for the activation of H_2 along this pathway (Figure 4). However, the entropy effect stabilizes the reactants more than the H−H activation TSs and puts the TSs a few kcal/mol higher than the Pd_5 + H_2 reactants. Therefore, we may expect a few kcal/mol entropy-related activation barrier for the first H_2 activation on the Pd_5 cluster. Later, after passing the H−H activation TS, a spin crossing occurs that turns the reaction to the singlet PES of the equatorial pathway and leads to the singlet-state final product **Pd5_1_c_(f,f′)**. The entire process is calculated to be exothermic by 20.5 and 11.0 kcal/mol in ΔH and ΔG, respectively.

C. Activation of the Second H_2. The activation of the second H_2 follows a pattern similar to that seen in the first H_2 case. The possibility of the coordination of the second H_2 molecule either to the axial or equatorial Pd atom of the tbp Pd_5 core in $Pd_5(H)_2$ gives rise to two distinct pathways. Those studied below involve the most stable $Pd_5(H)_2$ isomer, the singlet **Pd5_1_c_(f,f′)**, and the second most stable singlet $Pd_5(H)_2$ isomer **Pd5_1_c_(f,f)$_{eq}$** (cf. Figure 4).[26a,b]

First, let us consider the axial pathway. H_2 molecular coordination to the axial Pd atom of the lowest singlet $Pd_5(H)_2$, **Pd5_1_c_(f,f′)**, yields the **Pd5_2_a_(f,f′)** dihydrogen complex. However, we also found another axial complex, **Pd5_2_a_(e,f′)**, differing from **Pd5_2_a_(f,f′)** primarily by the binding site of the H^7 hydrogen ligand (edge vs face, Figure 5). Recall that the singlet **Pd5_1_c_(e,f′)** structure of the $Pd_5(H)_2$ reactant is not kinetically stable, as discussed in the preceding section. The two axial dihydrogen complexes are found to be of essentially the same stability. Indeed, according to Table 3, the calculated ΔH (ΔG) values of forming the **Pd5_2_a_(f,f′)** and **Pd5_2_a_(e,f′)** isomers of $Pd_5(H)_2(H_2)$ from the $Pd_5(H)_2$ + H_2 ground-state reactants (at 298.15 K) are −12.2 (−6.0) and −12.1 (−6.6) kcal/mol, respectively. Moreover, the **Pd5_2_a_(f,f′)** → **Pd5_2_a_(e,f′)** isomerization can be accomplished readily by the **Pd5_2_d1** transition state (Figure 5), with an associated barrier of only 0.4 kcal/mol (ΔH(298.15 K)) relative to **Pd5_2_a_(f,f′)** (Table 3). The IRC shows that the actual prereaction complex for the second H_2 activation is the **Pd5_2_a_(e,f′)** isomer.

Starting from the **Pd5_2_a_(e,f′)** complex, the activation of the H^8-H^9 bond occurs through the axial transition state **Pd5_2_b** and leads to the tetrahydride **Pd5_2_c_(t,t,e,f)** (Figures 5 and 6). In the **Pd5_2_b** TS, a noticeable change in geometry from that of **Pd5_2_a_(e,f′)** is the position of H^6, which moved down to the lower tetrahedron cap site with the concomitant rotation of the second H_2 unit to the symmetry plane of the former. TS **Pd5_2_b** is reachable from **Pd5_2_a_(e,f′)** with an activation barrier of $\Delta H^{\ddagger}$ (298.15 K) = 5.3 kcal/mol and is 6.8 kcal/mol below the $Pd_5(H)_2$ + H_2 asymptote. Similarly, with ΔG(298.15 K) calculations, the **Pd5_2_b** TS lies below this asymptote by 1.1 kcal/mol (Table 3). The formed intermediate **Pd5_2_c_(t,t,e,f)** can easily rearrange to the most favorable $Pd_5(H)_4$ product, **Pd5_2_c_(e,e,e,e)**, via the transition state **Pd5_2_d2**. As seen in Figure 5, this rearrangement is accompanied by a further shift of H^6 from the cap to the bridge site. The resultant

Pd5_2_c_(e,e,e,e) product of C_2 symmetry has its four hydrogen ligands positioned as the bridges of the Pd−Pd edges. In these bridge sites, the bond lengths of the unique Pd−H pairs are 1.659 and 1.699 Å and 1.672 and 1.747 Å. The $Pd_5(H)_2 + H_2 \rightarrow Pd_5(H)_4$ (**Pd5_2_c_(e,e,e,e)**) reaction is calculated to be exothermic by 18.7 kcal/mol in terms of ΔH(298.15 K) (Table 3). Because the isomerization transition state **Pd5_2_d2** lies 5.4 kcal/mol below the $Pd_5(H)_2 + H_2$ reactants, no overall enthalpy barrier is found for the activation of the second H_2 along this pathway (Figure 6).

We will now proceed to discuss the equatorial pathway. This term is assigned to the route initiated by forming the **Pd5_2_a_(f,f)$_{eq}$** complex via binding the second H_2 to the unique equatorial Pd^3 atom of the singlet **Pd5_1_c_(f,f)$_{eq}$** reactant (Figure 5). The corresponding $\Delta H(\Delta G)$ values of this equatorial H_2 coordination process at 298.15 K of −8.6 (−2.2) kcal/mol are ca. 3.5 (4.0) kcal/mol higher than the values calculated for the axial $Pd_5(H)_2(H_2)$ analogues (Table 3). H^8-H^9 bond activation takes place next through the equatorial transition state **Pd5_2_b′** and leads directly to the **Pd5_2_c_(e,e,f,f)$_{eq}$** product as verified by following the IRC (Figures 5 and 6). The activation barrier $\Delta H^{\ddagger}$(298.15 K) from **Pd5_2_a_(f,f)$_{eq}$** is 3.1 kcal/mol. However, the transition state **Pd5_2_b′** again falls below the $Pd_5(H)_2 + H_2$ reactants by 5.5 kcal/mol, meaning that there is no net activation barrier along this route. ΔG(298.15 K) results show a very small (1.4 kcal/mol) net barrier for this pathway (Table 3). In the **Pd5_2_c_(e,e,f,f)$_{eq}$** structure, the pairs of hydrogen ligands in the bridge and face sites share the equatorial Pd atom and the equatorial Pd−Pd edge, respectively. The overall reaction $Pd_5(H)_2 + H_2 \rightarrow Pd_5(H)_4$ (**Pd5_2_c_(e,e,f,f)$_{eq}$**) is exothermic by 16.0 kcal/mol (Table 3). Thus, the **Pd5_2_c_(e,e,f,f)$_{eq}$** isomer of $Pd_5(H)_4$ is only 2.7 kcal/mol less stable than the alternative-path isomer, **Pd5_2_c_(e,e,e,e)**, and is anticipated to rearrange to the latter at low energetic cost. The **Pd5_2_c_(e,e,f,f)$_{eq}$ → Pd5_2_c_(e,e,e,e)** isomerization is not expected to affect the mechanism of the $Pd_5(H)_2 + H_2 \rightarrow Pd_5(H)_4$ reaction and was not studied here. Isomers of the second H_2 activation product $Pd_5(H)_4$ are precursors for further hydrogenation steps of Pd_5 as discussed in detail below.

In passing, it is important to conclude that in contrast to our previous findings for smaller clusters Pd_3 and Pd_4[10] the activation of the second H_2 by Pd_5 is predicted to be thermodynamically and kinetically favorable.

D. Formation of the $Pd_5(H)_4(H_2)$ Complex and Activation of the Third H_2. Parallel to the behavior revealed previously for $Pd_3(H)_2$ and $Pd_4(H)_2$,[10] the $Pd_5(H)_4$ species is also found to bind H_2 to give the $Pd_5(H)_4(H_2)$ dihydrogen complex. We have located six isomers of this complex, and the most stable one, **Pd5_3_a_(e,e,e,e)**, is shown in Figure 7 (others shown in Figure 1S of Supporting Information). Five of these show negative enthalpy and free-energy changes for the $Pd_5(H)_4 + H_2 \rightarrow Pd_5(H)_4(H_2)$ reaction at 298.15 K (Table 3). For the most stable isomer **Pd5_3_a_(e,e,e,e)**, derived from the **Pd5_2_c_(e,e,e,e)** precursor, these ΔH (ΔG) values are −10.8 (−4.1) kcal/mol relative to the $Pd_5(H)_4 + H_2$ reactants. In the **Pd5_3_a_(e,e,e,e)** structure, the third H_2 molecule is bound to the equatorial Pd^2 site.

The activation of the third H_2 molecule via the reaction $Pd_5(H)_4 + H_2 \rightarrow Pd_5(H)_6$ is an endothermic process, as seen in Table 3. The energetically most favorable isomers of the $Pd_5(H)_6$ product, **Pd5_3_c_(e,e,e,e,e,e)** and **Pd5_3_c_(e,e,f,f,f,f)**, are higher in enthalpy by 5.4 and 9.1 kcal/mol (at 298.15 K), respectively, than the reactants **Pd5_2_c_(e,e,e,e)** + H_2. Note that upon the formation of **Pd5_3_c_(e,e,e,e,e,e)** equatorial ring Pd^3-Pd^4 bond cleavage takes place. Transition states involved in this activation have not been examined because the $Pd_5(H)_4 + H_2 \rightarrow Pd_5(H)_6$ reaction is endothermic.

E. Reaction/Adsorption of Additional H_2 Molecules with the $Pd_5(H)_4(H_2)$ Complex. On the basis of our previous study of $Pd_n + xH_2$ reactions for $n = 3$ and 4,[10] further hydrogen adsorption is anticipated to occur on the hydrogen-unsaturated Pd centers of the $Pd_5(H)_4(H_2)$ complex. Indeed, the latter can bind several additional H_2 molecules to form $Pd_5(H)_4(H_2)_m$ complexes successively with $m = 2-5$, all containing the $Pd_5(H)_4$ "dissociatively adsorbed core" of either **Pd5_2_c_(e,e,e,e)** or **Pd5_2_c_(e,e,f,f)$_{eq}$**. A large number of $Pd_5(H)_4(H_2)_m$ structures were calculated (Table 4 and Figures 2S−4S of Supporting Information), of which only the most energetically favorable ones are given in Figure 7.

For $m = 2$, we have found nine different isomers, eight of which exhibit negative enthalpy and free-energy changes relative to $Pd_5(H)_4 + 2H_2$ at 298.15 K (Table 4). The global minimum for $m = 2$, **Pd5_4_a_(e,e,e,e)** of C_2 symmetry, features two molecularly bound H_2 in the equatorial sites of the $Pd_5(H)_4$ core and has ΔH(298.15 K) = −22.2 and ΔG(298.15 K) = −7.9 kcal/mol relative to the values for $Pd_5(H)_4 + 2H_2$. For $m = 3$, we have located 10 distinct isomers. According to Table 4, the enthalpy and free-energy changes at 298.15 K with respect to $Pd_5(H)_4 + 3H_2$ are negative for all of these isomers. Among the $Pd_5(H)_4(H_2)_3$ isomers, **Pd5_5_a_(e,e,e,e)** and **Pd5_5_a′_(e,e,e,e)**, differing by the position of one of the molecularly adsorbed H_2 (axial vs equatorial), are calculated to be the most stable and are almost degenerate. Namely, the enthalpy and free-energy changes of forming the $Pd_5(H)_4(H_2)_3$ complex from $Pd_5(H)_4 + 3H_2$ at 298.15 K are found to be −29.3 and −8.8 kcal/mol, respectively, and −29.5 and −8.1 kcal/mol for isomers **Pd5_5_a_(e,e,e,e)** and **Pd5_5_a′_(e,e,e,e)**, respectively. For $m = 4$, six structures have been located, again all with negative enthalpy and free-energy changes relative to the values for $Pd_5(H)_4 + 4H_2$ at 298.15 K (Table 4). The global minimum for $m = 4$ is **Pd5_6_a_(e,e,e,e)**, having C_2 symmetry featuring two axially and two equatorially bound H_2 to the $Pd_5(H)_4$ core. The calculated ΔH(298.15 K) and ΔG(298.15 K) values of the process $Pd_5(H)_4 + 4H_2 \rightarrow$ **Pd5_6_a_(e,e,e,e)** are −37.0 and −8.9 kcal/mol, respectively. Finally, with $m = 5$, we have found the hydrogen-saturated tbp Pd_5 clusters, structures **Pd5_7_a_(e,e,e,e)** and **Pd5_7_a_(e,e,f,f)$_{eq}$**. The former structure (Figure 7) represents the most favorable arrangement of two dissociatively and five molecularly adsorbed H_2 on the tbp Pd_5, with ΔH(298.15 K) and ΔG(298.15 K) values relative to $Pd_5(H)_4 + 5H_2$ being −43.2 and −8.2 kcal/mol, respectively (Table 4). The latter isomer of $Pd_5(H)_4(H_2)_5$ appears to be ca. 2−3 kcal/mol less stable because the respective numbers are −40.0 and −6.4 kcal/mol.

Thermodynamic values for the reaction $Pd_5(H)_4 + mH_2 \rightarrow Pd_5(H)_4(H_2)_m$ ($m = 1-5$) at 298.15 and 70 K are shown in Figure 8, where the lowest-energy product structures are taken for each m. The main conclusions that can be extracted from this Figure parallel those drawn previously for the analogous hydrogenation reactions involving $Pd_n(H)_2$ ($n = 3$ and 4) dissociative complexes.[10] In particular, as Figure 8 clearly shows, at 70 K the entropy contribution to ΔG is significantly diminished relative to that at 298.15 K. At 298.15 K, the free energy of reaction is nearly independent of the value of m up to $m = 5$ and is around −9 kcal/mol. This indicates that the incremental stabilization is nearly zero and that the adsorption of the additional H_2 molecules on $Pd_5(H)_4$ is "neutral" in free energy or takes place without free-energy loss or gain. At lower

temperature (70 K), the heats of reaction ΔH are calculated to be −10.3, −21.3, −28.0, −35.2, and −41.1 kcal/mol, and ΔG(70 K) are −9.0, −18.4, −23.9, −29.6, and −34.1 kcal/mol for $m = 1-5$, respectively. This puts the incremental values of ΔH(70 K) values for the $Pd_5(H)_4(H_2)_{m-1} + H_2 \rightarrow Pd_5(H)_4(H_2)_m$ ($m = 1-5$) process of the molecular adsorption of consecutive H_2 at −10.3, −11.0, −6.7, −7.2, and −5.9 kcal/mol, which can be compared with ΔG(70 K) values of −9.0, −9.4, −5.5, −5.7, and −4.5 kcal/mol for $m = 1-5$, respectively.

IV. Conclusions

In this article, we have presented the results of DFT B3LYP calculations on the successive hydrogenation steps of the trigonal bipyramidal (tbp) Pd_5 cluster to form hydrogen-rich species observed experimentally in the gas phase.[4] Our findings based on the in-depth exploration of the respective PESs and computed thermodynamic values can be summarized as follows:

(1) Tbp-like isomers of the bare Pd_5 cluster in the triplet state are found to be its energetically most favorable forms.

(2) In the first hydrogenation step, the H_2 molecule becomes at first molecularly bound to form $Pd_5(H_2)$, in which the H−H bond is activated to form the $Pd_5(H)_2$ dihydride. Similar to the process for Pd_3 and Pd_4,[10] this occurs in a spin-forbidden process, $Pd_5(\text{triplet}) + H_2 \rightarrow Pd_5(H)_2$ (singlet). A spin crossing is expected to move the reaction onto the singlet PES of the equatorial activation pathway. The overall reaction to give the most stable dissociative product, **Pd5_1_c_(f,f′)**, is exothermic by 20.5 kcal/mol in terms of ΔH(298.15K). The latter species features both hydrogens at cap sites of the nonadjacent faces of tbp Pd_5.

(3) In the second hydrogenation step, the next H_2 becomes bound to form $Pd_5(H)_2(H_2)$, where the H−H bond is activated to give the $Pd_5(H)_4$ tetrahydride. Two pathways have been found with a negative net activation enthalpy of the process $Pd_5(H)_2 + H_2 \rightarrow Pd_5(H)_4$ leading to distinct isomers of the product, **Pd5_2_c_(e,e,e,e)** and **Pd5_2_c_(e,e,f,f)$_{eq}$**, which is exothermic by 18.7 and 16.0 kcal/mol, respectively. It is suggested that the higher reactivity of Pd_5 toward H_2 compared to that of Pd_3 and Pd_4 observed in the kinetic studies[4] might be caused by the availability of the favorable second H_2 activation channels in the Pd_5 cluster, which are nonexistent for the smaller $Pd_{3,4}$ clusters.[10]

(4) The activation of the third H_2 via the $Pd_5(H)_4 + H_2 \rightarrow Pd_5(H)_6$ reaction is endothermic by at least 5.5 kcal/mol and is not likely to take place.

(5) After the activation (dissociative adsorption) of the first two H_2 molecules has been completed, subsequent steps of the hydrogenation of Pd_5 take place via molecular adsorption onto the $Pd_5(H)_4$ tetrahydride, ultimately leading to the hydrogen-saturated cluster $Pd_5(H)_4(H_2)_5$. The latter exhibits a H/Pd ratio of 2.8, which is in accord with that extracted from Figure 4 of ref 4.[27] A large number of stable (even at $T = 298.15$ K) non-hydrogen-saturated species $Pd_5(H)_4(H_2)_m$ ($m = 1-4$) containing the $Pd_5(H)_4$ core structure are also predicted for each m.

Acknowledgment. J.M. acknowledges the Emerson Center for a Visiting Fellowship and thanks the staff of the Emerson Center for kind help and for the use of the computer facilities and programs. The present research is supported in part by grants (CHE-9627775 and CHE-0209660) from the National Science Foundation. We acknowledge the Cherry L. Emerson Center of Emory University. Our use of its resources is in part supported by a National Science Foundation grant (CHE-0079627) and an IBM Shared University Research Award.

Supporting Information Available: Cartesian coordinates of all of the structures discussed in the paper. Isomeric structures of the third H_2 activation product, $Pd_5(H)_6$, and the $Pd_5(H)_4(H_2)_m$ complexes for $m = 1-5$. This material is available free of charge via the Internet at http://pubs.acs.org.

References and Notes

(1) Arakawa, H.; Aresta, M.; Armor, J. N.; Barteau, M. A.; Beckman, E. J.; Bell, A. T.; Bercaw, J. E.; Creutz, C.; Dinjus, E.; Dixon, D. A.; Domen, K.; DuBois, D. L.; Eckert, J.; Fujita, E.; Gibson, D. H.; Goddard, W. A.; Goodman, D. W.; Keller, J.; Kubas, G. J.; Kung, H. H.; Lyons, J. E.; Manzer, L. E.; Marks, T. J.; Morokuma, K.; Nicholas, K. M.; Periana, R.; Que, L.; Rostrup-Nielson, J.; Sachtler, W. M. H.; Schmidt, L. D.; Sen, A.; Somoriai, G. A.; Stair, P. C.; Stults, B. R.; Tumas, W. *Chem. Rev.* **2001**, *101*, 953.

(2) See, for example, (a) Wicke, E.; Brodowsky, H. In *Hydrogen in Metals*; Alefeld, G., Völkl, J., Eds.; Springer: Berlin, 1978; Vol. 2, p 73. (b) Farias, D.; Schilbe, P.; Patting, M.; Rieder, K.-H. *J. Chem. Phys.* **1999**, *110*, 559 and references therein. (c) Okuyama, H.; Siga, W.; Takagi, N.; Nishijima, M.; Aruga, T. *Surf. Sci.* **1998**, *401*, 344. (d) Behm, R. J.; Christmann, K.; Ertl, G. *Surf. Sci.* **1980**, *99*, 320.

(3) Efremenko, I.; Sheintuch, M. *Surf. Sci.* **1998**, *414*, 148 and references therein.

(4) Fayet, P.; Kaldor, A.; Cox, D. M. *J. Chem. Phys.* **1990**, *92*, 254.

(5) (a) Thomas, J. M. *Angew. Chem., Int. Ed. Engl.* **1988**, *27*, 1673. (b) Thomas, J. M. *Angew. Chem., Int. Ed. Engl.* **1994**, *33*, 913. (c) Cox, D. M.; Fayet, P.; Brickman, R.; Hahn, M. Y.; Kaldor, A. *Catal. Lett.* **1990**, *4*, 271.

(6) See, for example, Knickelbein, M. B.; Koretsky, G. M.; Jackson, K. A.; Pederson, M. R.; Hajnal, Z. *J. Chem. Phys.* **1998**, *109*, 10692 and references therein.

(7) For a comprehensive set of the representative references, the reader is referred to our previous paper.[10]

(8) Cui, Q.; Musaev, D. G.; Morokuma, K. *J. Chem. Phys.* **1998**, *108*, 8418.

(9) Cui, Q.; Musaev, D. G.; Morokuma, K. *J. Phys. Chem. A* **1998**, *102*, 6373.

(10) Moc, J.; Musaev, D. G.; Morokuma, K. *J. Phys. Chem. A* **2000**, *104*, 11606.

(11) (a) Becke, A. D. *Phys. Rev. A* **1988**, *38*, 3098. (b) Lee, C.; Yang, W.; Parr, R. G. *Phys. Rev. B* **1988**, *37*, 785. (c) Becke, A. D. *J. Chem. Phys.* **1993**, *98*, 5648.

(12) Hay, P. J.; Wadt, W. R. *J. Chem. Phys.* **1985**, *82*, 299.

(13) Dunning, T. H., Jr. *J. Chem. Phys.* **1970**, *53*, 2823.

(14) Andrae, D.; Haussermann, U.; Dolg, M.; Stoll, H.; Preuss, H. *Theor. Chim. Acta* **1990**, *77*, 123.

(15) Dunning, T. H., Jr. *J. Chem. Phys.* **1989**, *90*, 1007. Note that d functions on H were excluded from the correlation-consistent basis set.

(16) (a) Gonzalez, C.; Schlegel, H. B. *J. Chem. Phys.* **1989**, *90*, 2154. (b) Gonzalez, C.; Schlegel, H. B. *J. Phys. Chem.* **1990**, *94*, 5523.

(17) The choice of low temperature (70 K) was explained in our previous work.[10] Note that the actual cluster temperature in the experiment by Cox et al.[4] was not reported.

(18) Frisch, M. J.; Trucks, G. W.; Schlegel, H. B.; Scuseria, G. E.; Robb, M. A.; Cheeseman, J. R.; Zakrzewski, V. G.; Montgomery, J. A., Jr.; Stratmann, R. E.; Burant, J. C.; Dapprich, S.; Millam, J. M.; Daniels, A. D.; Kudin, K. N.; Strain, M. C.; Farkas, O.; Tomasi, J.; Barone, V.; Cossi, M.; Cammi, R.; Mennucci, B.; Pomelli, C.; Adamo, C.; Clifford, S.; Ochterski, J.; Petersson, G. A.; Ayala, P. Y.; Cui, Q.; Morokuma, K.; Malick, D. K.; Rabuck, A. D.; Raghavachari, K.; Foresman, J. B.; Cioslowski, J.; Ortiz, J. V.; Stefanov, B. B.; Liu, G.; Liashenko, A.; Piskorz, P.; Komaromi, I.; Gomperts, R.; Martin, R. L.; Fox, D. J.; Keith, T.; Al-Laham, M. A.; Peng, C. Y.; Nanayakkara, A.; Gonzalez, C.; Challacombe, M.; Gill, P. M. W.; Johnson, B. G.; Chen, W.; Wong, M. W.; Andres, J. L.; Head-Gordon, M.; Replogle, E. S.; Pople, J. A. *Gaussian 98*, revision A.1; Gaussian, Inc.: Pittsburgh, PA, 1998.

(19) Fahmi, A.; van Santen, R. A. *J. Phys. Chem.* **1996**, *100*, 5676.

(20) Bertani, V.; Cavallotti, C.; Masi, M.; Carra, S. *J. Phys. Chem. A* **2000**, *104*, 11390. In this B3LYP study, the trigonal bipyramidal triplet was reported to be the lowest-energy structure for Pd_5 with equatorial and axial Pd−Pd edges of 3.05 and 2.61 Å, respectively.

(21) Dai, D.; Balasubramanian, K. *Chem. Phys. Lett.* **1999**, *310*, 303. Jahn−Teller distortion of the tbp triplet ($^3E'$) structure was not considered by these authors.

(22) Our calculated (BSII) atomization energy of the most stable tbp **Pd_5(1)** of 146.1 kcal/mol can be compared with the MRSDCI (MRSDCI + Q)[21] values of 146 (161) kcal/mol.

(23) LaJohn, L. A.; Christiansen, P. A.; Ross, R. B.; Atashroo, T.; Ermler, W. C. *J. Chem. Phys.* **1987**, *87*, 2812.

(24) (a) With the BSII basis set, the enthalpy change for the axial **Pd5_1_b** (**Pd5_1_b** (^{3}A)) TS falls below that of **Pd5_1_c_(t, t)$_{ax}$** (**Pd5_1_c_(t, t)$_{ax}$** (^{3}A)) (Figure 4), thus the latter intermediate might not correspond to stable species. Similarly, the **Pd5_1_d2** isomerization TS becomes lower in enthalpy than the **Pd5_1_c_(e, f)$_{eq}$** dihydride when the BSII basis set is used, so this $Pd_5(H)_2$ singlet isomer might not be a stable species either. (b) With the BSII basis set, the equatorial **Pd5_1_b′** (^{3}A) TS becomes lower in enthalpy than the **Pd5_1_c_(t, t)$_{eq}$** (^{3}A) intermediate (Figure 4), so the latter might not correspond to a stable species. (c) Because of the shallowness of the PES in the direction of the imaginary mode of the **Pd5_1_d4** (^{3}A) TS, the IRC calculation generated only one point and stopped (both directions); this was followed by the geometry optimizations started at the indicated "forward" and "backward" IRC structures.

(25) No stable triplet counterpart of **Pd5_1_c_(f, f)$_{eq}$** has been found, and the most stable triplet **Pd5_1_c_(f, f)$_{ax}$** structure collapsed eventually to **Pd5_1_c_(e, e)$_{eq}$** ($^3A_2$).

(26) (a) Although the interconversion between these two species has not been studied, the related energetic barrier is expected to be relatively small on the basis of both the results of the preceding section for the **Pd5_1_c_(f, f)$_{ax}$ → Pd5_1_c_(f, f′)** rearrangement and calculated interconversion barriers for the $Pd_4(H)_2$ isomers.[10] (b) The triplet $Pd_5(H)_2(H_2)$ dihydrogen complexes formed by H_2 coordination to the axial and equatorial sites of the most stable triplet $Pd_5(H)_2$ reactant, **Pd5_1_c_(e, e)$_{eq}$** ($^3A_2$), have been found (at the geometry-optimization level) to be 9.1 and 7.7 kcal/mol less favorable, respectively, than the most stable singlet complex of this type, **Pd5_2_a_(f, f′)**.

(27) Strictly speaking, the agreement concerns those experimental conditions where "D_2 is injected into the reactor". Cox et al. reported a slightly higher D/Pd ratio for the case "in which D_2 is entrained in the primary helium gas and exposed to the laser initiated plasma".[4]